



Basal Plane Delamination Energy Measurement in a Ti_3SiC_2 MAX Phase

ORIOLO GAVALDA-DIAZ,^{1,2} JACK LYONS,¹ SIYANG WANG,¹
MAX EMMANUEL,¹ KATHARINA MARQUARDT,¹ EDUARDO SAIZ,¹
and FINN GIULIANI¹

1.—Department of Materials, Centre of Advanced Structural Ceramics, Imperial College London, London SW7 2AZ, UK. 2.—e-mail: o.gavalda-diaz@imperial.ac.uk

The {0001} basal plane delamination dominating the crack-wake bridging in MAX phases at a bulk scale has been investigated by studying the small-scale fracture of a Ti_3SiC_2 . In situ micro-double cantilever beam (DCB) tests in a scanning electron microscope were used to grow a stable crack along the basal plane, measure the fracture energy, and study the crack propagation mechanism at the nanoscale. The results show that the fracture energy (10–50 J/m²) depends on small misorientations angles (e.g., 5°) of the basal plane to the stress field. This induces permanent deformation which can be observed once the DCB has been unloaded. The nanoscale study of the crack shows that the plasticity at the crack tip is small, but a number of pairs of dislocations are forming at each side of the crack. Hence, this study helps to explain the enhanced fracture energy values and possible sources of energy dissipation in basal plane delamination, which is the one of the main toughening mechanisms in the bulk fracture of MAX phases.

INTRODUCTION

$\text{M}_{n+1}\text{AX}_n$ phases ($n = 1, 2, \text{ or } 3$) are a family of materials comprised of nanolaminate tertiary carbides and nitrides,^{1–4} where M is an early transition metal, A is an A group metal (typically groups 13–16) and X is carbon or nitrogen. These materials contain M_{n+1}X_n layers which have strong covalent bonds interleaved with pure A layers, with weaker M–A bonds.⁵ This combination gives the MAX phases a unique set of properties combining both metallic and ceramic traits. The properties of the MAX phases have been widely studied in recent years. Like ceramics, they are lightweight, stiff, and chemically stable; however, they are also damage-tolerant, show pseudo-ductility, and are readily machinable like metals.^{3,6} This unique set of properties is attributed to their nano-layered structure and hexagonal crystal structure ($\text{P6}_3/\text{mmc}$ space group), with a highly symmetric unit cell and a large c/a ratio. This leads to a high degree of

anisotropy and a lack of the five independent slip systems required for typical plastic crystal deformation.^{7,8}

The main deformation and fracture mechanisms in MAX phases at room temperature are activation of basal slip, kink band formation, and delamination along the basal plane.^{9–11} Once the kink bands are formed, basal plane delamination will dominate crack-wake bridging in MAX phases. Fracture toughness values ranging from 6.5 to 16 $\text{MPa}\sqrt{\text{m}}$ for different MAX phases, such as Ti_3SiC_2 , Ti_3AlC_2 , and Ti_2AlC , have been reported in the literature.⁸ Gilbert et al.¹² studied the R-curve in a Ti_3SiC_2 MAX phase with different grain sizes. They observed high levels of crack-wake bridging in the fractured surface, inducing a rise from 8.5–11 $\text{MPa}\sqrt{\text{m}}$ to 14–16 $\text{MPa}\sqrt{\text{m}}$ after a few millimetres (2–4 mm) of crack propagation. The latest values were believed to be the highest reported for a monolithic, single-phase, non-transforming ceramic.⁸ Gilbert et al.¹² also commented that the high fracture toughness was in part due to crack bridging by the heavily delaminated lamellae.

In this work, we measure the energy required for basal plane fracture in a Ti_3SiC_2 MAX phase in order to better understand the intrinsic toughening mechanisms observed at a bulk scale. We used a scanning electron microscope (SEM; FEG-SEM, Quanta; FEI, USA) in situ micro-double cantilever beam (DCB) fracture test to propagate a controlled and stable crack along the basal plane. With this set-up, we measured the strain energy release rate stored in the beams at different crack lengths, and, by using the Griffith's failure criteria,¹³ we obtained the critical energy release rate. This test permits an accurate measurement of the delamination and fracture energies that can be used to determine the energy dissipation mechanisms at the nanoscale, and how they influence the macro-scale response.

EXPERIMENTAL METHODOLOGY

Material Processing and Sample Preparation

Coarse-grained Ti_3SiC_2 was produced using an analogous method to that described by Barsoum et al.¹⁴ to create highly orientated large-grain Ti_3SiC_2 . The precursor mix was produced under an argon atmosphere using commercially available products: titanium (-325 mesh, 99%; Alfa Aesar, UK), silicon (-325 mesh, 99.5%; Alfa Aesar), and carbon (>99.9%; Sigma Aldrich, UK). Carbon was used in the form of graphite powder. The atomic ratio in the precursor mix was 3:1:1.95 (Ti:Al:C) to compensate for the carbon uptake from the graphite crucible and the environment. The powder mix was ball-milled (Planetary Ball miller Pm100; Retsej, Germany), for 180 min using 10-mm-diameter ZrO_2 -milling media in a sealed nylon jar at 150 rpm to break up agglomerates and homogenize the powder. The precursor powder was precompact in a 14-mm die under uniaxial pressure (60 MPa). The preform was then placed into a graphite die (28 mm), capped, and lined with graphite film. The die was then placed into a hot press (HP W/25/1furnace; FCT Systeme, Germany) and heated under vacuum to 1450°C for 8 h. The sample was cooled to room temperature inside the hot press, before being reheated to 1300°C under argon. Once up to temperature, the load was applied (35 MPa). The temperature was raised from 1300°C to 1400°C for 1 h, then subsequently raised to 1600°C for 24 h under load and finally allowed to cool naturally back to room temperature. The sample surface was mechanically ground (Accutom-100; Struers, USA) and polished (METASERV 2000 Grinder Polisher, Buehler, USA) and then finally vibropolished (VibroMetTM 2 Vibratory Polisher; Buehler) using Buehler's MasterPolishTM Alumina suspensions.

Characterization

Electron backscatter diffraction (EBSD) was used to identify the MAX phase grains with the

desired crystal orientation: the basal plane nearly perpendicular ($\pm 2^\circ$) to the sample surface. EBSD scanning was carried out using SEM equipped with an EBSD camera (eFlashHR v2; Bruker, Germany) using 30-kV electron beam voltage. Collection and analysis of the EBSD data were conducted using the Bruker ESPRIT 2.1 software. We recorded the Euler angles [$\varphi_1, \Phi, \varphi_2$] for crystals with desirable orientation. This allows the fabrication of DCBs inside grains with $\Phi = 90 \pm 2^\circ$ and the aligning of the basal plane with the notch in-plane based on φ_1 .

Micromechanical Testing

The focused ion beam milling of the DCBs consisted of several stages all executed at 30 kV and with the sample placed normal to the focused ion beam column. The current was reduced as the fabrication proceeded, trenching with currents of 7 nA, 3 nA, and 500 pA to create a sufficiently large trench around the DCB, and to reduce the cross-sectional area of the DCB. Finally, a notch was cut using a line scan at 10 pA. The notch acts as a stress concentrator to initiate the crack. Between each step, an image correlation alignment procedure was used to correct the beam shift due to current changes and stage drift. The final DCB geometry had nominal dimensions of 8–10 μm height, 2 μm width and 6 μm thickness.

The DCB splitting tests were carried out within an SEM equipped with an in situ nanoindenter (Alemnis, Switzerland). A 60° wedge tip with a length of 10 μm was used to split the DCB at a displacement rate of 2 nm/s.

The Mode I critical energy release rate (G_I^c) or fracture energy when the hexagonal single crystal is oriented with the basal plane parallel to the axial direction of the split, was calculated using the following equation:^{15,16}

$$G_I^c = \frac{3E_{11}\delta^2w^3}{4(a+\chi w)^4} \left[1 + (1+\nu_{13}) \left(\frac{w}{(a+\chi w)} \right)^2 \right], \quad (1)$$

where δ and w are the displacement and width of the beams, respectively, and a , the crack length. All these values are measured from the SEM image frames. χ is a correction factor that takes account of rotation at the crack tip. Due to the transverse isotropic nature of the Ti_3SiC_2 , it can be defined based on the elastic constants as:¹⁶

$$\begin{aligned} \chi &= \sqrt{\frac{a_{66}}{11a_{11}}} \sqrt{3 - 2 \left(\frac{\Gamma}{1+\Gamma} \right)^2}, \quad \text{with } \Gamma \\ &= 1.18 \frac{a_{66}}{\sqrt{a_{11}a_{22}}}, \end{aligned} \quad (2)$$

where $a_{11} = 1/E_{11}$, $a_{22} = 1/E_{33}$, and $a_{66} = 1/G_{13}$. Using the compliance matrix modeled for the β -polytype Ti_3SiC_2 ,¹⁷ the elastic coefficients calculated for this work are listed in Table I.

Table I. Elastic coefficients: Young's modulus (E), shear modulus (G) and Poisson's ratio (ν) obtained using the stiffness matrix modeled for the β -polytype Ti_3SiC_2 17

	$E_{11} = E_{22}$ (GPa)	E_{33} (GPa)	G_{12} (GPa)	$G_{13} = G_{23}$ (GPa)	ν_{12}	$\nu_{13} = \nu_{23}$
β - Ti_3SiC_2	346	337	145	121	0.194	0.161

For the transversely isotropic HCP crystal structure, 1 and 2' are two orthogonal in-(basal) plane directions and 3 corresponds to the $\langle 0001 \rangle$ direction (c -axis).

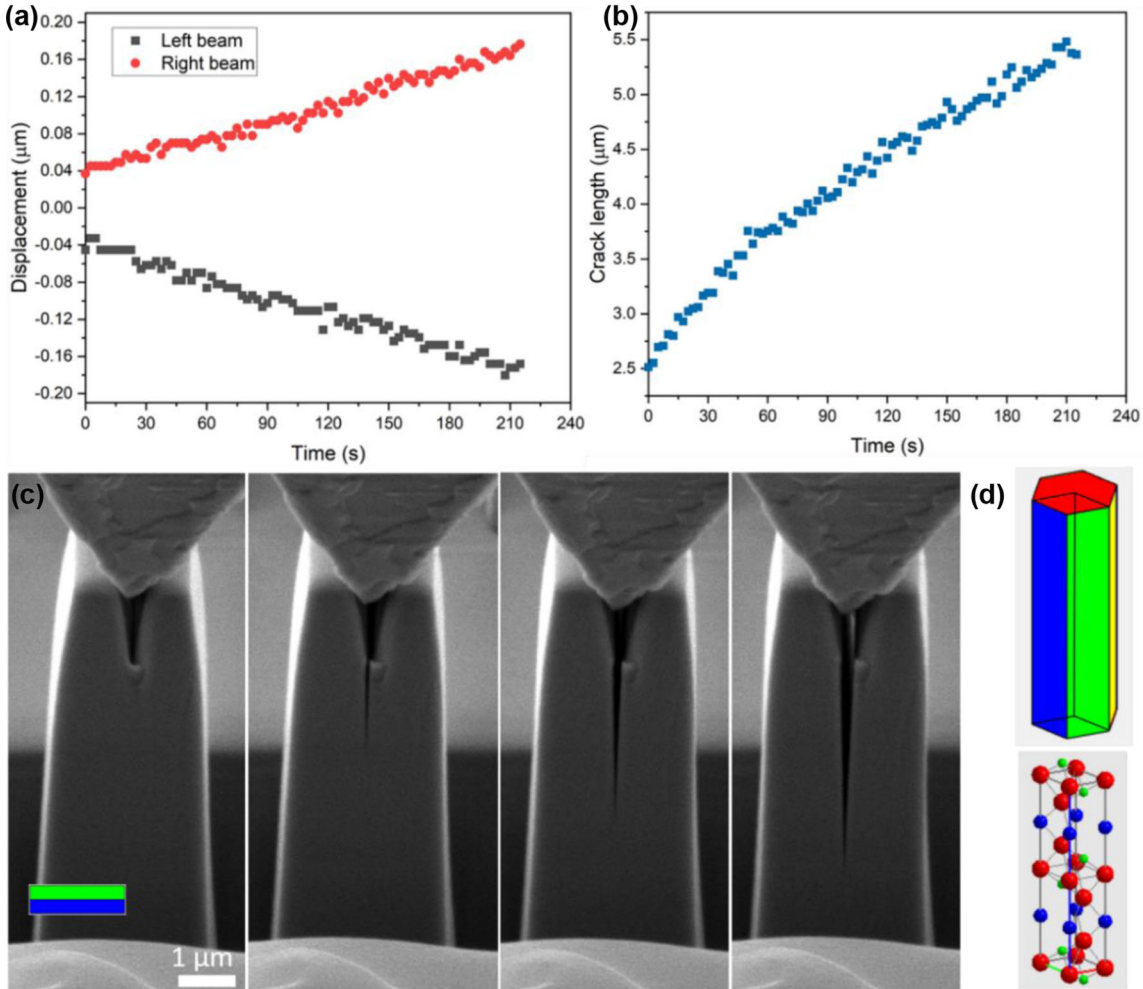


Fig. 1. (a) Displacement of the left and right beams and (b) crack length over time measured via image tracking from the SEM frames obtained during the splitting. (c) SEM frames showing the crack propagation at different instants of the test, with the *inset* showing the unit cell representation of a Ti_3SiC_2 crystal orientation, oriented with respect to the viewing angle (movie available in the supplementary information). (d) A perspective view of the unit cell used in (c) which will be used to reference the crystal orientation.

RESULTS

The opening of the beams, the crack length, and SEM image frames over time (Fig. 1a–c, respectively) show the stable crack propagation achieved on the Ti_3SiC_2 DCB. The crack propagated straight along the DCB following the direction of the basal plane (as shown with the unit cell of the hexagonal

structure recreated from EBSD data in the inset in Fig. 1c) for more than 5 μm over 210 s. Figure 1d shows a perspective view of the hexagonal crystal lattice and unit cell used to describe the orientation in the experiments presented in this work.

Using the beam displacement and crack length data, the evolution of the fracture energy or critical energy release rate in Mode I (G_I^c) with crack length

was measured for four different Ti_3SiC_2 DCBs, all of them with the basal plane aligned along the splitting direction (see Fig. 2). There is a major difference between the values of critical energy release rate measured for the different DCBs: DCB 1 showed an average $G_1^c = 10 \pm 2 \text{ J/m}^2$, while for the others (DCB 2, 3, and 4), the average values were around 4–5 times larger: $G_1^c = 44 \pm 5 \text{ J/m}^2$.

Figure 3a–c show the top, front, and back face, respectively, for DCB 1 after being split. The crack originates from the notch in both faces and runs almost perfectly straight down the DCB. On the other hand, when looking at the others DCBs (Fig. 3c–e show DCB 2 as an example), it can be seen that, in the back face, the crack did not originate from the notch. This results in a basal plane not being perfectly aligned with the stress field. From the top images of DCB 1 and DCB 2, we measured a misalignment of $\approx 1^\circ$ for DCB 1 and $\approx 5^\circ$ for the other DCBs (compare the white dashed lines in Fig. 3a and d). Furthermore, it is also noticeable how, in the case of DCB 1, the residual opening of the beams (after the load has been removed) is considerably smaller than in the case of DCB 2. The white arrows in Fig. 3b and e indicate the residual opening measured at the notch tip, and which is 0.05 and 0.2 μm for DCB 1 and DCB 2, respectively.

Transmission electron microscope (TEM) analysis of the crack in DCB 1 (Fig. 4a and b) shows how the crack propagated along the basal plane with no major evidence of a large plastic volume ahead of the crack tip. Nevertheless, it seems that pairs of dislocations might be forming symmetrically in both sides of the crack every $\approx 100 \text{ nm}$ (see red circles in Fig. 4a). On the other hand, TEM analysis of the crack opening (behind the crack tip) from the DCBs, where the values of critical energy release rate were higher (Fig. 4c and d), shows that the affected area

becomes larger as there are multiple delamination events. The thickness of the affected area is more than 20 nm. Moreover, capturing the crack tip in these tests becomes more challenging as the opening of the beams is higher and the crack plane is slightly misaligned with the DCB surface.

DISCUSSION

Two main trends in the values of the critical energy release rate along the basal plane when splitting Ti_3SiC_2 DCBs have been measured in this work. In the case of DCB 1, the crack propagates within one basal plane and we measured a delamination energy of $10 \pm 2 \text{ J/m}^2$. For the other tests (DCB 2, 3, and 4), we observed multiple delamination events with higher values of fracture energy $\approx 44 \pm 5 \text{ J/m}^2$. This difference has been shown to be related to a misorientation of the basal plane with the stress field, which has been confirmed by looking at the different faces of the DCB after each test. The TEM analysis of the crack also shows that the area and number of basal planes affected increase when there is a small misorientation (5°). This conclusion can also be confirmed by looking at the residual opening of the beams after the load is removed: in DCB 1, the residual opening is considerably smaller than in the other DCBs (0.05 μm and 0.2 μm , respectively). Hence, propagating a crack with a small misorientation induces multiple delamination effects caused by different initiation points. These events are not reversible and induce a permanent deformation to the material.

The delamination energy measured ($10 \pm 2 \text{ J/m}^2$) is higher than the cleavage energy predicted via DFT of 2.81 J/m^2 , assuming that the crack propagates along the $\text{Ti}_1\text{-Si}$ plane as suggested in the literature¹⁸ (see Table II). This shows that some extra energy dissipation occurs during delamination. Based on the TEM analysis, we have observed that pairs of dislocations forming at each side of the crack might be absorbing extra energy if they are moving as the crack progresses (Fig. 4a).

If we compare the delamination energy to the values obtained when splitting 6H-SiC¹⁵ (see Table II) we notice that, in SiC, the cleavage energy measured experimentally is closer to that estimated via DFT ($5.95 \pm 1.79 \text{ J/m}^2$ and $8.15 \pm 0.44 \text{ J/m}^2$, respectively). This suggests that there is no permanent damage and that all the energy goes into forming the two surfaces. This effect can be supported by comparing the residual opening of the Ti_3SiC_2 and SiC DCBs after removing the wedge: the Ti_3SiC_2 DCB beams do not recover the original position (see Fig. 5a and b), while the SiC beams close the cracked surfaces back together (see Fig. 5c).

The data obtained suggest that the fracture in Ti_3SiC_2 will not be dominated by splitting a single basal plane, as small misalignments have already been shown to induce multiple delamination events.

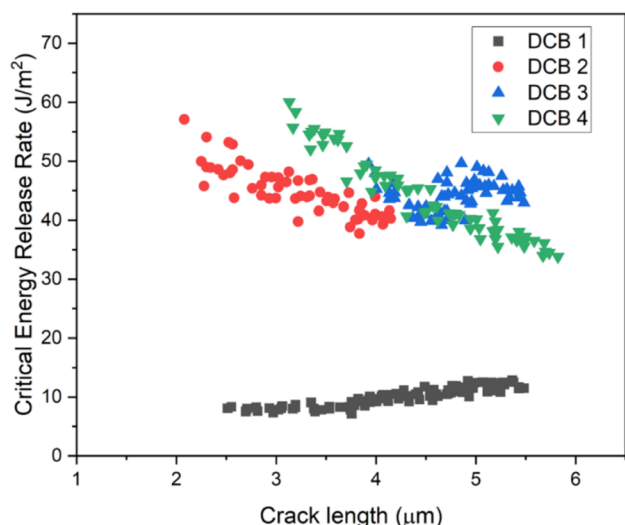


Fig. 2. Values of critical energy release rate (G_1^c) over crack length obtained for four different Ti_3SiC_2 DCBs, all oriented with the basal plane (0001) aligned with the splitting direction.

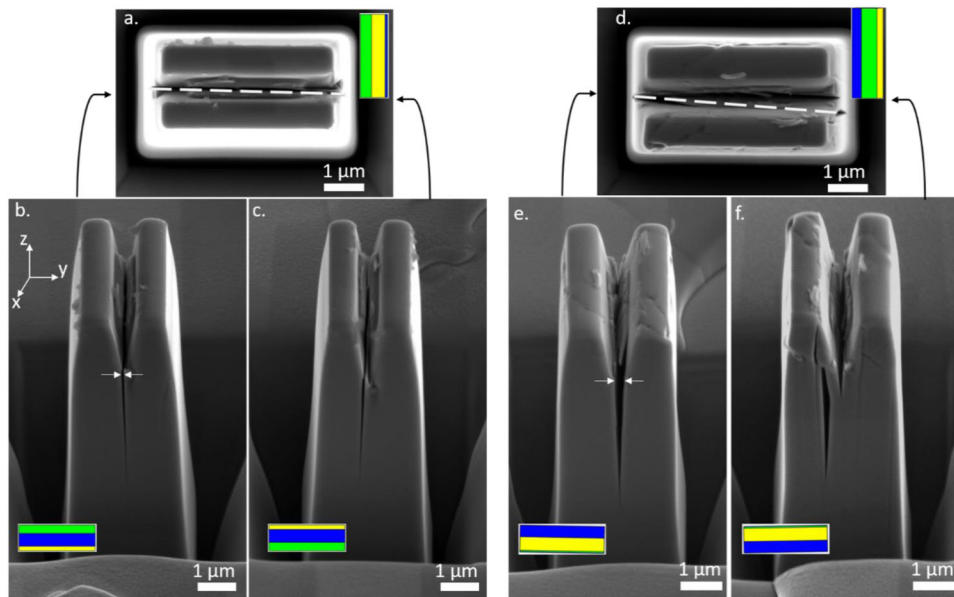


Fig. 3. DCBs after splitting with the tip retracted showing the top, front, and back faces for DCB 1 (a, b and c) and for DCB 2 (d, e, and f), respectively. The dashed lines in (a) and (d) show the misalignment of the basal plane with the stress field in the X–Y plane. The white arrows in (b) and (e) show the residual opening at the notch tip. The unit cell represents the Ti_3SiC_2 crystal orientation.

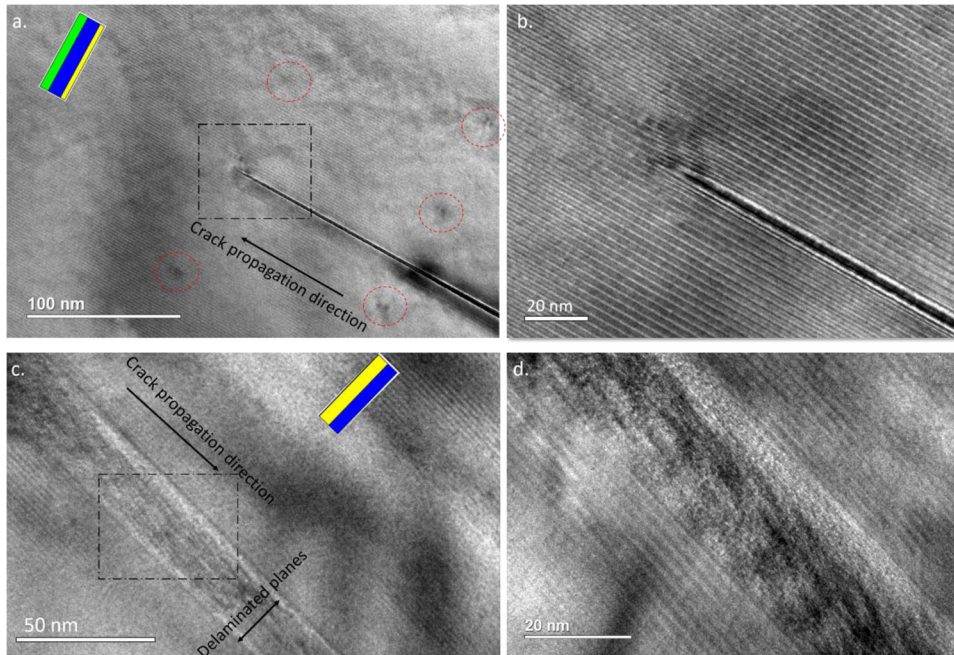


Fig. 4. Bright field TEM image of (a) the crack tip and pair of dislocations forming on each side of the crack (red circles) in the DCB 1 and (b) shows the magnified area highlighted in (a). Bright field TEM image of (c) split area (after $\approx 3\text{--}4\ \mu\text{m}$ of crack propagation) in the DCB 4 showing the affected area with delaminated planes, and (d) shows the magnified area highlighted in (c).

For samples in which several basal planes delaminated, we measured a fracture energy of $44 \pm 5\ \text{J/m}^2$. The results measured with macroscale testing in the literature¹² show a fracture toughness of 8.5–11 $\text{MPa}\sqrt{\text{m}}$ ($200\text{--}350\ \text{J/m}^2$) for short crack lengths. These results are still considerably higher than the values that we get in this work. However, our test shows that, differently from other monolithic

ceramics, basal plane fracture in MAX phases can lead to an intrinsic toughening mechanism which will have an impact on the fracture energy measured at a bulk scale.

The presented data help to explain the enhanced fracture toughness observed in MAX phases when compared to other ceramic materials. As mentioned in the Introduction, basal plane delamination acts

Table II. Literature values of cleavage and delamination energy obtained via density functional theory (DFT) and experimentally, and values of fracture energy obtained experimentally

	DFT			Experimental	
	Cleavage energy 2γ (J/m^2)			Cleavage energy (J/m^2)	Bulk fracture energy G^c (J/m^2)
6H-SiC		8.15 ± 0.44 ¹⁵		5.95 ± 1.79 ¹⁵	20–25 ¹⁹
Ti_3SiC_2	Ti ₁ -Si	Ti ₂ -C	Ti ₁ -C	≈ 10 ± 2 ^a (this work)	200–350 (short crack lengths) ¹²
	2.81 ¹⁸	5.44 ¹⁸	6.50 ¹⁸		

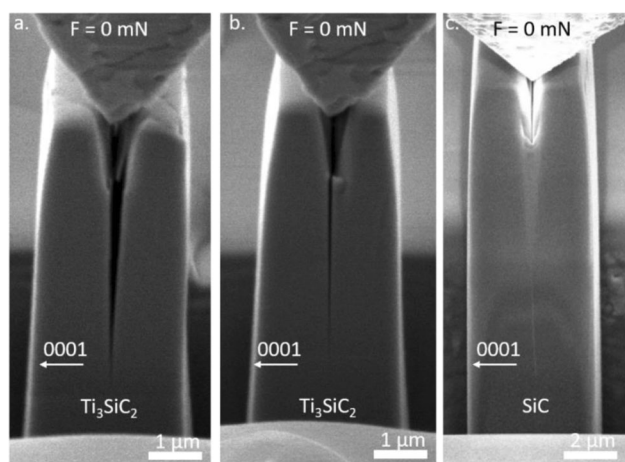
^aDelamination energy.

Fig. 5. SEM frames showing the permanent opening after the load has been removed observed in the Ti_3SiC_2 DCBs: (a) DCB 2 and (b) DCB1 compared to (c), the one observed in previous work on 6H-SiC¹⁵ ($F = 0$ mN).

as main source of crack-wake bridging. However, here we show how small misorientations of the basal plane respect to the stress field can produce higher values of fracture energy ($44 \pm 5 \text{ J/m}^2$) when compared to the delamination energy. Considering that in this test we propagate a crack for a few microns ($4\text{--}5 \mu\text{m}$), we believe that this is a significant source of intrinsic toughening that helps explain why the bulk fracture of this material can reach values up to 750 J/m^2 (or 16 MPa m).¹²

CONCLUSION

We have investigated the fracture of a Ti_3SiC_2 MAX phase by using an SEM in situ microscale DCB test. We achieved stable crack propagation along the basal plane. With this test, we have provided results of the delamination and fracture energies for a Ti_3SiC_2 MAX phase together with a nanoscale study of the sources of energy dissipation appearing during basal plane fracture. The results show that the delamination energy is $10 \pm 2 \text{ J/m}^2$,

but that small misorientations of the basal plane respect to the stress field give higher values of fracture energy ($44 \pm 5 \text{ J/m}^2$). This is caused by multiple delamination events happening simultaneously and inducing a permanent deformation to the material. Furthermore, even if the misalignment is reduced, we measured values of delamination energy higher than the surface energy expected for this material. This has been linked to a number of pairs of dislocations forming at each side of the crack.

ACKNOWLEDGEMENTS

The authors would like to acknowledge to the ESPRC MAP consortium (EP/POO6566/1) and the EPSRC Centre for Doctoral Training in Nuclear Energy: Building UK Nuclear Skills for Global Markets (EP/L015900/1).

CONFLICT OF INTEREST

The authors declare that they have no conflict of interest.

OPEN ACCESS

This article is licensed under a Creative Commons Attribution 4.0 International License, which permits use, sharing, adaptation, distribution and reproduction in any medium or format, as long as you give appropriate credit to the original author(s) and the source, provide a link to the Creative Commons licence, and indicate if changes were made. The images or other third party material in this article are included in the article's Creative Commons licence, unless indicated otherwise in a credit line to the material. If material is not included in the article's Creative Commons licence and your intended use is not permitted by statutory regulation or exceeds the permitted use, you will need to obtain permission directly from the copyright holder. To view a copy of this licence, visit <http://creativecommons.org/licenses/by/4.0/>.

SUPPLEMENTARY INFORMATION

The online version contains supplementary material available at <https://doi.org/10.1007/s11837-021-04635-9>.

REFERENCES

1. V.H. Nowotny, *Prog. Solid State Chem.* 5, 27. (1971).
2. W. Jeitschko, H. Nowotny, and F. Benesovsky, *J. Less-Common Met.* 7, 133. (1963).
3. M.W. Barsoum, and T. El-Raghy, *J. Am. Ceram. Soc.* 79, 1953. (1996).
4. M.W. Barsoum, *Prog. Solid State Chem.* 28, 201. (2000).
5. M. Magnuson, and M. Mattesini, *Thin Solid Films* 621, 108. (2017).
6. M.W. Barsoum, *Encycl. Mater. Sci. Technol. No. Table 1*, 1. (2000).
7. P.R. Howie, R.P. Thompson, S. Korte-Kerzel, and W.J. Clegg, *Sci. Rep.* 7(1), 1. (2017).
8. M.W. Barsoum, and M. Radovic, *Annu. Rev. Mater. Res.* 41(1), 195. (2011).
9. T. El-Raghy, A. Zavaliangos, M.W. Barsoum, and S.R. Kalidindi, *J. Am. Ceram. Soc.* 16, 513. (1997).
10. M.W. Barsoum, L. Farber, and T. El-Raghy, *Metall. Mater. Trans. A* 30(July), 1727. (1999).
11. J.M. Molina-Aldareguia, J. Emmerlich, J. Palmquist, U. Jansson, and L. Hutman, *Scr. Mater.* 49, 155. (2003).
12. C.J. Gilbert, D.R. Bloyer, M.W. Barsoum, A.P. Tomsia, and R.O. Ritchie, *Scr. Mater.* 42, 761. (2000).
13. B. Lawn, *Fracture of Brittle Solids*, 2nd edn. (Cambridge University Press, Cambridge, 1993).
14. M.W. Barsoum, and T. El-Raghy, *Metall. Mater. Trans. A* 30A, 363. (1999).
15. G. Sernicola, T. Giovannini, P. Patel, J.R. Kermode, D.S. Balint, T. Ben Britton, and F. Giuliani, *Nat. Commun.* <https://doi.org/10.1038/s41467-017-00139-w> (2017).
16. J.G. Williams, *Compos. Sci. Technol.* 35, 367. (1989).
17. N.I. Medvedeva, A.N. Enyashin, and A.L. Ivanovskii, *J. Struct. Chem.* 52(4), 785. (2011).
18. M. Higashi, S. Momono, K. Kishida, N.L. Okamoto, and H. Inui, *Acta Mater.* 161, 161. (2018).
19. J.L. Henshall, D.J. Rowcliffe, and J.W. Edington, *J. Am. Ceram. Soc.* 60, 373. (1977).

Publisher's Note Springer Nature remains neutral with regard to jurisdictional claims in published maps and institutional affiliations.